Functional Consequences of Neuromyelitis Optica-IgG Astrocyte Interactions on Blood-Brain Barrier Permeability and Granulocyte Recruitment[1]

Thierry Vincent,*† Philippe Saikali,† Romain Cayrol,‡ Alejandro D. Roth,†§ Amit Bar-Or,† Alexandre Prat,‡ and Jack P. Antel[2†]

Autoantibody neuromyelitis optica-IgG (NMO-IgG) recognizing aquaporin-4 (AQP4) is implicated as playing a central role in the physiopathology of NMO. The aim of this in vitro-based study was to characterize functional consequences of interaction between NMO-IgG and cells of the neurovascular unit (astrocytes and brain endothelium) that would provide insight into recognized features of NMO, namely altered blood-brain barrier (BBB) permeability and granulocyte recruitment. We used sera from NMO and longitudinally extensive transverse myelitis cases shown to bind in a characteristic perivascular pattern to primate cerebellar slices. Using flow cytometry, we found that sera from NMO-IgG-positive patients reacted with CNS-derived human fetal astrocytes, whereas sera from multiple sclerosis patients did not. We demonstrated that NMO-IgG binding to astrocytes alters aquaporin-4 polarized expression and increases permeability of a human BBB endothelium/astrocyte barrier. We further demonstrated that NMO-IgG binding to human fetal astrocytes can result in NK cell degranulation, astrocyte killing by Ab-dependent cellular cytotoxicity and complement-dependent granulocyte attraction through the BBB model. Our study highlights important functional roles for NMO-IgG that could account for pathological lesions and BBB dysfunction observed in NMO.

Neuromyelitis optica (NMO)[3] or Devic's disease is a recurrent disease of the CNS that affects mainly the optic nerves and spinal cord (1). NMO pathology is characterized by necrotic lesions with perivascular inflammatory infiltrates enriched in granulocytes. Ig deposition associated with products of complement activation suggests a pathogenic role of humoral-mediated immune mechanisms (1). A disease-specific serum autoantibody (NMO-IgG) has been shown to bind to structures adjacent to CNS microvessels, pia, subpia, and Virchow-Robin spaces (2). The target Ag has been identified as being aquaporin-4 (AQP4), the main water channel protein in the CNS (3). AQP4 is mainly expressed on astrocyte end-feet at the blood-brain barrier (BBB) and brain-cerebrospinal fluid barrier (4). Analyses of AQP4-deficient mice revealed its involvement in cerebral water and ion homeostasis regulation, astrocyte migration, neural signal transduction, and demonstrated its role for the maintenance of BBB integrity (5, 6).

A series of clinical and pathologic observations suggest that NMO-IgG plays a central role in the physiopathology of NMO: 1) plasma exchange can produce an early therapeutic response in NMO-IgG-positive patients (7–9); 2) the Ig deposition and activated complement components in NMO lesions are in a vasculocentric distribution corresponding to sites of high AQP4 expression (10–12); 3) AQP4 and glial fibrillary acidic protein (GFAP) immunoreactivity are lost in most of the NMO lesions, especially in active perivascular regions (12, 13); and 4) anti-AQP4 Ab titers correlate with the clinical and radiological severity of the disease and decrease after efficient treatment (14). Nevertheless, the mechanisms by which NMO-IgG contributes to disease pathogenesis remain to be defined. In this study, we assessed the functional effects of sera from NMO-IgG-positive patients on human primary astrocytes and brain endothelial cells (ECs), and defined novel functions on BBB permeability and granulocyte recruitment that could contribute to the development of the pathological features described in NMO.

Materials and Methods

Sera and Abs

We selected sera from seven adult patients (22–81 years of age) in whom NMO-IgG was detected by indirect immunofluorescence on primate cerebellum slides (Binding Site, Birmingham, U.K.), five patients with NMO, and two patient with longitudinally extensive transverse myelitis. Four of the NMO sera samples were assayed by the classical test on mice tissues described by the Mayo Clinic Neuroimmunology Laboratory (Rochester, MN), and NMO-IgG positivity was confirmed in all samples tested. Nine age-matched patients (age 29–55) with clinically definite multiple sclerosis (MS) and eight healthy subjects (age 24–65) were selected as control. Although meeting the diagnostic criteria for clinically definite MS, MS4

*Laboratoire d'Immunologie, Hôpital Saint-Eloi-CHU Montpellier, Montpellier, France; †Neuroimmunology Unit, and Experimental Therapeutics Program, Montreal Neurological Institute, McGill University, and ‡Neuroimmunology Research Laboratory, Centre Hospitalier de l'Université de Montréal–Notre-Dame Hospital, Université de Montréal, Montréal, Québec, Canada; and §Department of Biology, Faculty of Science, Universidad de Chile, Santiago, Chile

Received for publication April 28, 2008. Accepted for publication August 5, 2008.

The costs of publication of this article were defrayed in part by the payment of page charges. This article must therefore be hereby marked *advertisement* in accordance with 18 U.S.C. Section 1734 solely to indicate this fact.

[1] This study was supported by grants from the Canadian Institutes of Health Research, by the Multiple Sclerosis Society of Canada (MSSC) and by the Canadian Foundation for Innovation (to A.P., A.B.-O., and J.P.A.). A.B.-O. is recipient of the MSSC Don Paty Award and McGill Dawson Scholar. A.P. holds a Donald Paty Career Development Award of the MSSC and is a Research scholar from the Fond de la Recherche en Santé du Québec. P.S. and R.C. hold studentships from the MSSC and from the Neuroinflammation Training Program of the Canadian Institutes for Health Research.

[2] Address correspondence and reprint requests Dr. Jack P. Antel, Neuroimmunology Unit, Montreal Neurological Institute, McGill University, 3801 University Street, Montreal, Quebec H3A 2B4, Canada; E-mail address: jack.antel@mcgill.ca

[3] Abbreviations used in this paper: NMO, neuromyelitis optica; MS, multiple sclerosis; AQP4, aquaporin-4; HFA, human fetal astrocyte; BBB, blood-brain barrier; EC, endothelial cell; GFAP, glial fibrillary acidic protein; ADCC, Ab-dependent cellular cytotoxicity.

only presented bilateral brain stem lesions with no spinal cord or supratentorial lesions on one patient's magnetic resonance imaging scan and could possibly still develop into clinical NMO. All MS and healthy control sera samples were negative by indirect immunofluorescence on primate cerebellum slides. All patients gave informed consent, and all studies were approved by the ethics committee of McGill University following Declaration of Helsinki principles. Anti-AQP4 was purchased from Alomone Laboratories, FITC-conjugated goat anti-human IgG from Jackson Immunoresearch Laboratories, PE-conjugated anti-CD107a, FITC-conjugated anti-MHC class I, and goat anti-rabbit Ig from BD Biosciences, anti-von Willebrand factor VIII from DakoCytomation, Alexa Fluor 488-conjugated anti-GFAP, Alexa Fluor 594 goat anti-rabbit, and Alexa Fluor 633 goat anti-mouse Abs from Molecular Probes, PE-conjugated anti-human, Cy3-conjugated and nonconjugated anti-GFAP Abs from Sigma-Aldrich and FITC-conjugated anti-rabbit Ab from Chemicon International.

Human primary cells

Human fetal astrocytes (HFAs) were isolated as previously described (15) from human CNS tissue from fetuses at 17–23 wk of gestation obtained from the Human Fetal Tissue Repository (Albert Einstein College of Medicine, Bronx, NY) following Canadian Institutes for Health Research-approved guidelines. Cultures were determined to be >90% pure (16). Human BBB-derived ECs (BBB-ECs) were isolated from CNS tissue obtained from temporal lobe resections from young adults undergoing surgery for the treatment of intractable epilepsy, as previously described (17, 18).

Immunofluorescence

Primate cerebellum sections (The Binding Site) or primary cells grown on Thermanox coverslips (Nunc) were fixed in 4% paraformaldehyde for 10 min, washed in PBS and blocked for 1 h in HHGB (HBSS containing 10% goat serum, 2% horse serum, 2% FBS, 1 mM HEPES buffer, and 0.1% sodium azide). For intracellular staining, cells were permeabilized in PBS containing 0.5% Triton X-100 at room temperature for 15 min. After incubation with primary Abs and diluted sera (1/50) overnight at 4°C in blocking solution, the substrates were washed in PBS, labeled at room temperature with species specific fluorescent secondary Abs in blocking solution, washed in PBS, incubated 30 min with TO-PRO-3 (Invitrogen) for nuclear staining, mounted in Prolong antifade mounting medium (Molecular Probes), and examined with a Leica TCS 4D confocal scanning microscope.

Flow cytometry analysis

HFAs were detached using PBS containing 1 mM EDTA, incubated with anti-MHC class I Ab or test human sera (1/50) in FACS buffer (PBS containing 1% FCS and 0.1% sodium azide), washed and incubated with PE-labeled goat anti-human Ab. Intracellular staining was performed by fixing and permeabilizing the cells for 10 min at room temperature with paraformaldehyde/saponin buffer (4% (w/v) paraformaldehyde, 0.1% (w/v) saponin, and 10 mM HEPES in HBSS). After washes with saponin buffer (0.1% (w/v) saponin in FACS buffer), cells were incubated with Alexa Fluor 488-conjugated anti-GFAP Ab. Isotypes matched for concentration of primary Abs were used for all stainings. Cells were washed, fixed in 1% formaldehyde containing PBS, and analyzed on a FACSCalibur (BD Biosciences).

Isolation of human NK cells and granulocytes

Venous blood was drawn from normal volunteer donors in agreement with institutional guidelines. PBMCs were isolated using Ficoll-Hypaque density gradient centrifugation (GE Healthcare), and NK cells were subsequently purified using allophycocyanin-conjugated anti-NKP46 Abs and anti-allophycocyanin MACS beads (Miltenyi Biotec) following the manufacturer's instructions. Cells obtained ($CD3^-$ $NKP46^+$) were >95% pure. Granulocytes were prepared by density centrifugation using Polymorphprep (Axis-Shield), according to the manufacturer's instructions. Cells obtained were >90% pure.

CD107a mobilization assay

CD107a mobilization assay was done as previously described (19). NK cells (effector) were used at an E:T ratio of 1:1 with HFAs (target) preincubated for 1 h in culture medium containing 10% of patient or control sera. After washes, HFAs were left in 100 μl of medium to which was added 100 μl of NK cells, 1 μl of 2 mM monensin, and 1 μl of PE-conjugated CD107a Ab or concentration-matched isotype control IgG1-PE. After 5 h at 37°C, cells were washed and analyzed on a FACSCalibur.

^{51}Cr release assays

HFAs were plated in 96-well plates and incubated overnight at 37°C with 1–10 μCi/well of ^{51}Cr (MP Biomedicals). After washes, HFAs were preincubated 1 h in culture medium containing 10% of patient or healthy control sera. After washes, NK cells were added at an E:T ratio of 1:1 and incubated for 4 h at 37°C. HFA lysis was assessed by radioactivity measurement in a gamma counter (Matrix 9600; Canaberra Packard) as previously described (20). Fc receptor blockade on effector cells was performed by preincubating NK cells for 1 h at 37°C with 50 μg/ml polyclonal human IgG (Caltag Laboratories). Serum IgG depletion was performed using HiTrap protein G HP columns (GE Healthcare) according to the manufacturer's instructions.

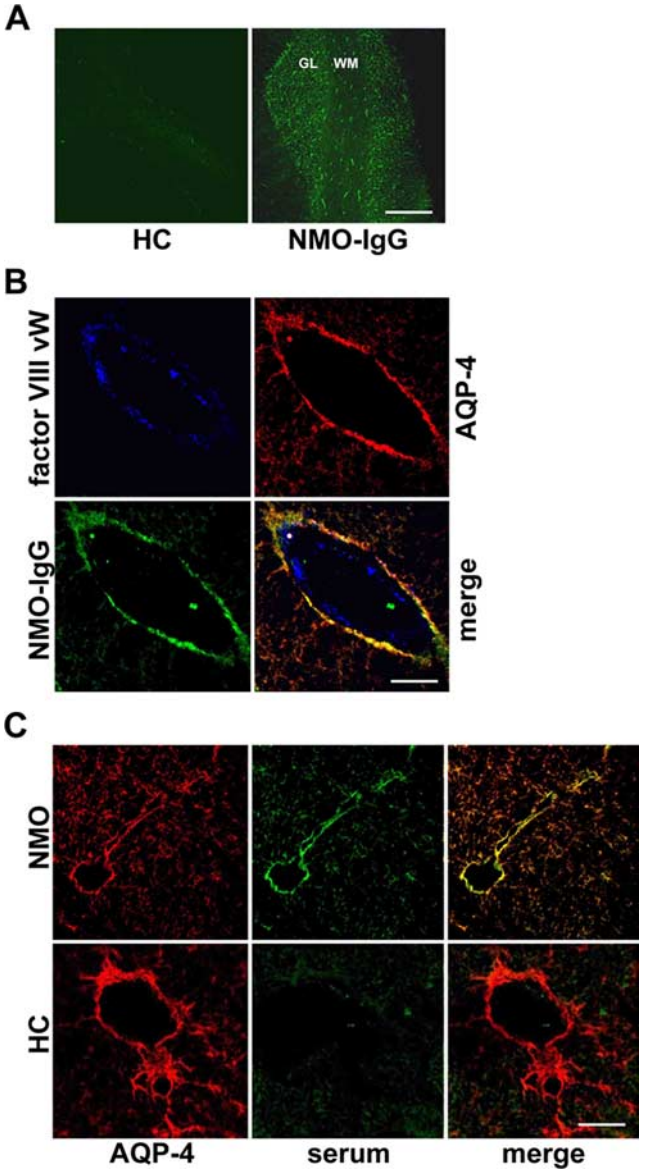

FIGURE 1. NMO-IgG binds primate CNS tissues. *A*, Indirect immunofluorescence pattern of NMO-IgG binding to primate cerebellum (*right*) features linear perivascular staining prominent in the white matter (WM) and the granular layer (GL). Healthy control (HC) subject serum (*left*) was used as a negative control. Scale bar represents 200 μm. *B*, Endothelium of cerebellum white matter was immunostained with mouse anti-von Willebrand factor VIII (blue). Confocal microscopy images show that binding of NMO-IgG (green) is external to endothelium and colocalizes with AQP4 (red). Scale bar represents 50 μm. *C*, Dual immunofluorescence of cerebellum white matter microvessels stained with rabbit anti-AQP4 (red) and NMO-IgG-positive (*top*, green) or healthy control (*bottom*, green) sera demonstrates colocalization of binding of NMO sera and anti-AQP4 Ab. Scale bar represents 50 μm.

Permeability assays

BBB-ECs and HFAs were used to generate an in vitro model of the human BBB. HFAs were plated on the bottom side of the Transwell filter insert of

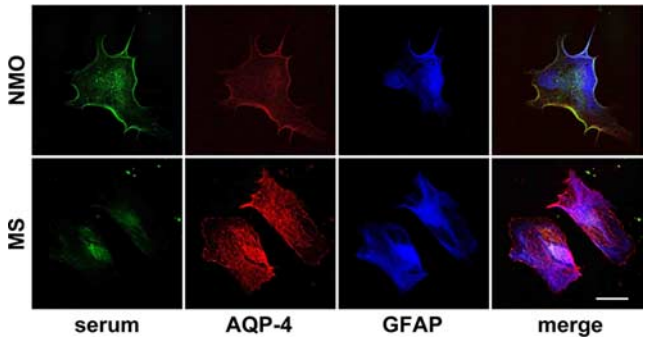

FIGURE 2. Indirect immunofluorescence staining of primary HFAs. Confocal microscopy shows that NMO-IgG (*top*, green) binds to the plasma membrane of GFAP-positive (blue) cultured HFAs and colocalizes with AQP4 (red). MS patient serum (*bottom*) was used as negative control. Scale bar represents 25 μm.

a gelatin-coated 3-μm pore size Boyden chambers (BD Biosciences) positioned upside down in EC culture medium and allowed to adhere for 1 h. The insert was inverted and placed in a 24-well cell culture plate. On day 3, BBB-ECs were plated on the topside of the insert. On day 6, 5% patient or control sera were added to both chambers. FITC-BSA (Invitrogen) (50 μg/ml) was added to the upper chambers and its diffusion across the BBB model was monitored using a FL600 microplate fluorescent reader (BioTek). BBB permeability was calculated using the following formula, as previously published (21): (BSA lower chamber) $\times$ 100/(BSA upper chamber).

Chemotaxis assays

HFAs were plated in 24-well plates and BBB-ECs were plated on the Transwell filter insert of gelatin-coated 3-μm pore size Boyden chambers. On day 3, HFAs were incubated 1 h in culture medium containing 10% of patient or control sera. After washes, 10% of fresh serum was added in the lower chamber as a source of complement and purified granulocytes were added into the upper chamber. When mentioned, complement was inactivated in the added fresh serum by heating 1 h at 56°C. After 2 h, granulocytes that had migrated through the EC was counted in the lower chamber, stained with an anti-CD107a Ab and analyzed by flow cytometry. Sera used as a source complement were tested in our FACS binding assay to exclude the presence of unspecific anti-astrocyte Abs.

Statistical analyses

Data handling and analysis were performed using Prism 3.0 (GraphPad Software). Due to small sample size, non-parametric tests (two-tailed Mann-Whitney tests) were used to compare the reactivity of sera derived from the total NMO, MS, and healthy controls (see Figs. 3, 5, and 6). For remaining experiments (see Figs. 4 and 7) in which serum samples were selected from a homogeneous larger population of healthy controls or MS

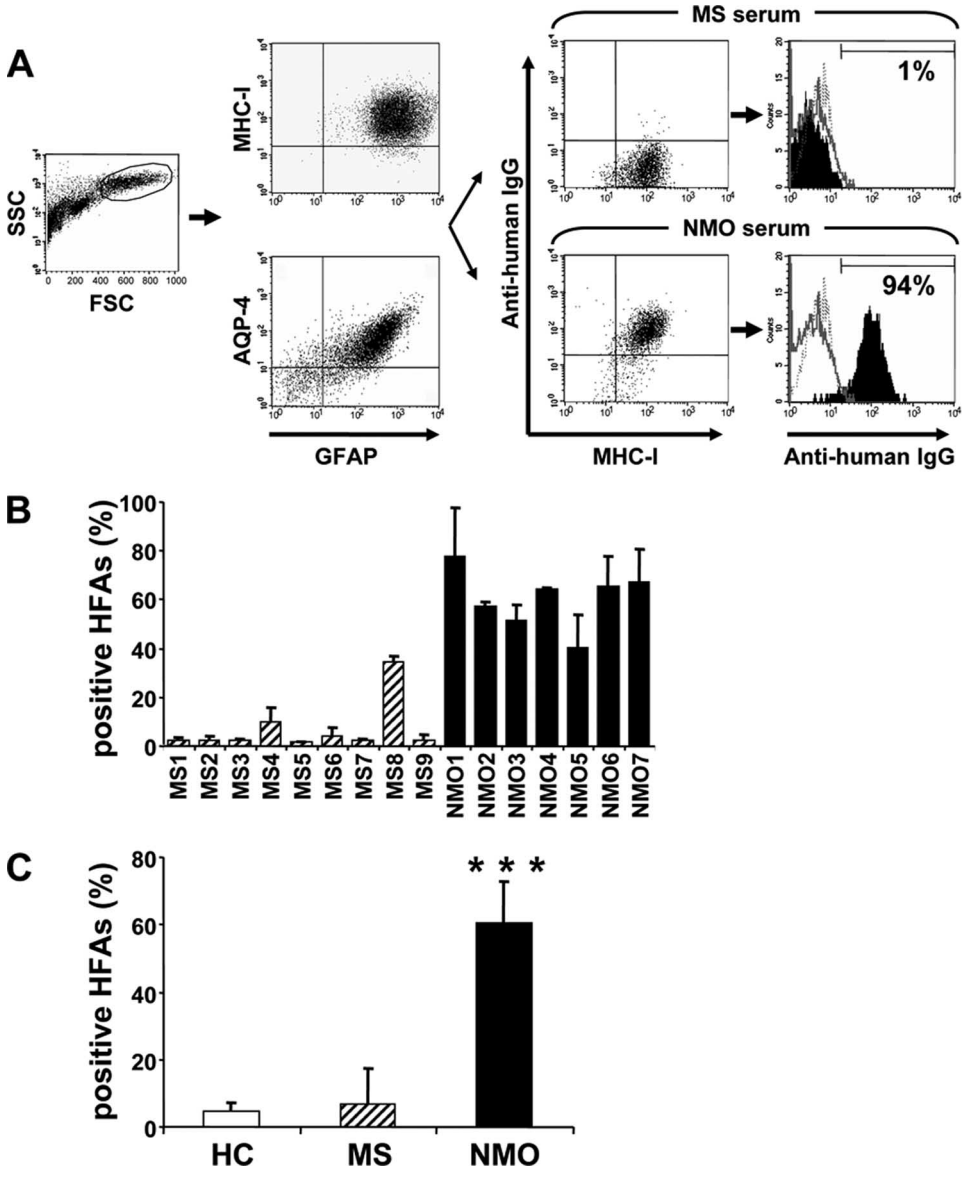

FIGURE 3. Specific binding of NMO-IgG to HFAs. *A*, Forward and side scatter (FSC/SSC) dot plot of HFAs (*left panel*). Cells gated in the *left panel* express GFAP, AQP4, and MHC class I (*middle panels*). Results of combined staining of MHC class I cells (HFAs) with NMO, MS, or healthy control (HC) serum followed by PE-conjugated anti-human IgG (*right panels*). The dot plots in the *left column* of *right* side indicates the immunoreactivity of HFAs with NMO but not MS donor serum. Histograms shown at *far right* indicate the high percentage of HFAs reactive with NMO and not MS serum (filled histogram). Binding by healthy control serum (gray line histogram) and the isotype control values (dotted histogram) are shown. *B*, Percentage of positive HFAs obtained with sera from seven NMO-IgG-positive patients (■) and nine sex- and age-matched MS patients (▨). Data shown are mean ± SD of three independent experiments. *C*, Mean percentage ± SD of HFA-positive cells obtained with sera from NMO-IgG-positive patients compared with healthy controls or MS patients. ***, $p < 0.001$.

patients (i.e., all negative for anti-AQP4 Abs) and NMO patients (i.e., all positive for anti-AQP4 Abs), parametric statistic tests were applied. Permeability curves (see Fig. 4) were evaluated with repeated-measures two-way ANOVA followed by a Bonferroni posttest comparing all pairs of data points. All data points are expressed as mean from at least $n = 3$ experiments, each conducted in duplicate. Granulocyte recruitment (see Fig. 7) results were compared using a Student's t test.

Results

NMO-IgGs bind primate CNS tissue

To ascertain that NMO-IgGs bind primate CNS tissues in similar pattern as in rodent tissues (2, 3), we tested five NMO and two longitudinally extensive transverse myelitis patients' sera by indirect immunofluorescence on sections of normal primate cerebellum. We observed the characteristic perivascular staining pattern previously described for rodent tissues (2); staining was prominent in the white matter and the granular layer where microvascular elements are the most abundant (Fig. 1*A*). Dual immunostaining with anti-AQP4 Ab and NMO sera showed that the Ag recognized by NMO-IgGs colocalized with the AQP4 at the BBB around the capillary endothelium (Fig. 1*B*). No specific staining was observed with MS or healthy control subject sera (Fig. 1, *A* and *C*).

NMO-IgGs specifically bind primary HFA

We first demonstrated by confocal microscopy that primary HFAs express AQP4 and are recognized by NMO-IgG (Fig. 2). The NMO-IgG binding colocalizes with AQP4 Ab labeling at the membrane of HFAs. Sera from healthy control subjects or MS patients produced only nonspecific intracellular staining. Flow cytometry analysis confirmed that HFAs, identified as GFAP- and MHC class I-positive cells, are recognized both by a commercially available anti-AQP4 Ab and by NMO-derived sera, but not by MS sera (Fig. 3*A*). We found that sera from all seven NMO-IgG-positive patients stained the surface of HFAs (Fig. 3*B*); mean percentage of HFAs stained was significantly increased in the NMO sera group when compared with MS sera or to healthy control sera ($61 \pm 12\%$ vs $6.8 \pm 10.7\%$ and $4.8 \pm 2.2\%$ respectively; $p < 0.0001$) (Fig. 3*C*). Under similar staining conditions, there was no significant binding of NMO sera or anti-AQP4 Ab to neurons (data not shown).

NMO-IgGs alter AQP4 polarization to astro-endothelial synapses and disrupt BBB permeability

To address whether NMO-IgG binding could alter BBB function, we used an in vitro model of the BBB in which HFAs were grown above a monolayer of human BBB-derived ECs (BBB-ECs). In contrast to HFAs grown on a plastic substrate where such cells are large with few and short extensions (Fig. 4*A*, *left*), HFAs cultured in contact with BBB-ECs present a smaller cell body and extend long processes (Fig. 4*A*, *right*). We could show by confocal immunofluorescence that whereas AQP4 appeared regularly distributed on the membrane of HFAs in monoculture, it displayed a polarized expression at the end of HFA processes when cocultured with BBB-ECs (Fig. 4*B*). To investigate the effect of NMO-IgG binding on AQP4 expression, HFA BBB-EC cocultures were incubated for 24 h in the presence of 10% of NMO-IgG-positive sera. Although the level of AQP4 expression on astrocytes did not change significantly (assessed by FACS, data not shown), the pattern of expression was markedly altered, giving rise to an intracellular and punctate immunostaining pattern with decreased AQP4 expression on the astrocyte processes (Fig. 4*B*), probably indicating an internalization of AQP4 molecules in intracytoplasmic vacuoles. Incubation with healthy control sera did not alter the polarized AQP4 expression (Fig. 4*B*).

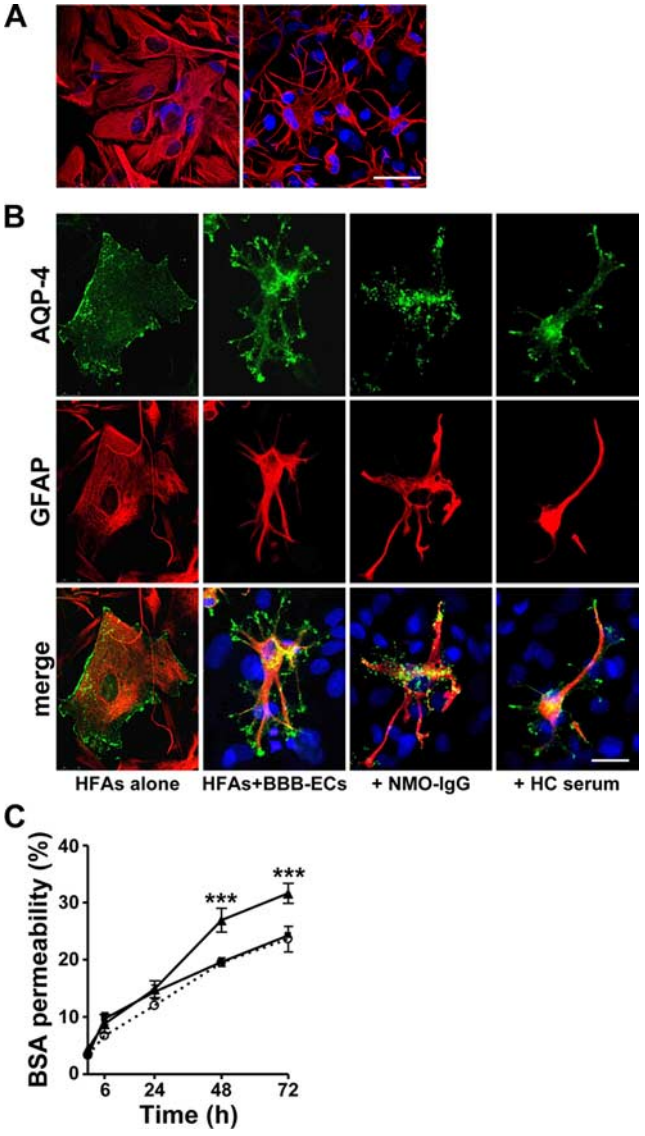

FIGURE 4. NMO-IgGs induce AQP4 internalization and BBB permeabilization. *A*, HFAs cultured alone (*left*) or above a monolayer of BBB-ECs (*right*) were immunostained with anti-GFAP Ab (red) and with nuclear stain TO-PRO-3 (blue). Morphologic changes of HFAs from cells with large cell bodies and limited processes to cells with smaller cell bodies and more extended processes. Scale bar represents 50 μm. *B*, Confocal microscopy of HFAs grown alone or above a monolayer of BBB-ECs and then incubated for 24 h with 10% NMO-IgG or healthy control (HC) sera. Cells were immunostained with anti-GFAP (red) and anti-AQP4 (green) Abs and with nuclear stain TO-PRO-3 (blue). Coculturing HFAs with BBB-ECs results in polarization of AQP4 to HFA end-feet. NMO-IgG disrupts AQP4 polarization and induces its internalization, an effect not seen with healthy control sera. Scale bar represents 25 μm. *C*, Human BBB-ECs and HFAs were grown on alternate sides of Boyden chamber membranes and treated with culture medium containing either 5% NMO-IgG-positive (▲), MS (■), or healthy control (○) sera. Permeability of the BBB model to FITC-BSA is substantially increased in the presence of NMO-IgG when compared with MS or healthy contol sera treated BBB-ECs. Data shown are mean results ± SD from three sera samples per group in duplicate. ***, $p < 0.001$.

To assess the effect of altered AQP4 expression on BBB permeability, we applied NMO-IgG-positive sera to cocultures of human BBB-ECs and HFAs, grown on alternate sides of a Boyden chamber membrane, our in vitro BBB model. Five percent (final concentration) of test sera were added in both the upper and the

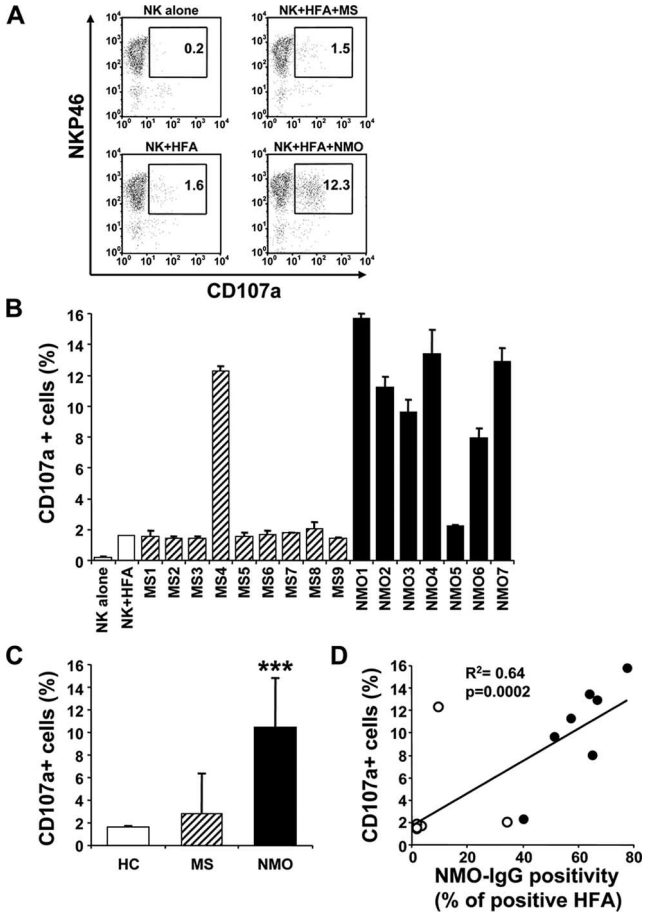

FIGURE 5. HFA-bound NMO-IgGs induce NK cell degranulation. *A*, Representative FACS profile showing increased proportion of NK cells ($NKP46^+$) that express CD107a following a 4-h coculture with HFAs that had been preincubated for 1 h with an NMO donor serum compared with cocultures with HFAs alone or HFAs preincubated with an MS donor serum sample. *B*, Percentage of NK cells positive for CD107a membrane expression obtained with sera from seven NMO-IgG-positive (■) and nine sex- and age-matched MS patients (▨). Data shown are mean ± SD of triplicate wells. *C*, Mean ± SD of CD107a-positive NK cells obtained with NMO-IgG-positive sera compared with healthy control or MS patient sera. ***, $p < 0.001$. *D*, Correlation between the extent of HFA directed reactivity of NMO or MS sera (as the percentage of HFAs with bound IgG and the percentage of CD107a-positive NK cells after coculture with HFAs preincubated with NMO-IgG-positive sera (●) or MS (○) sera).

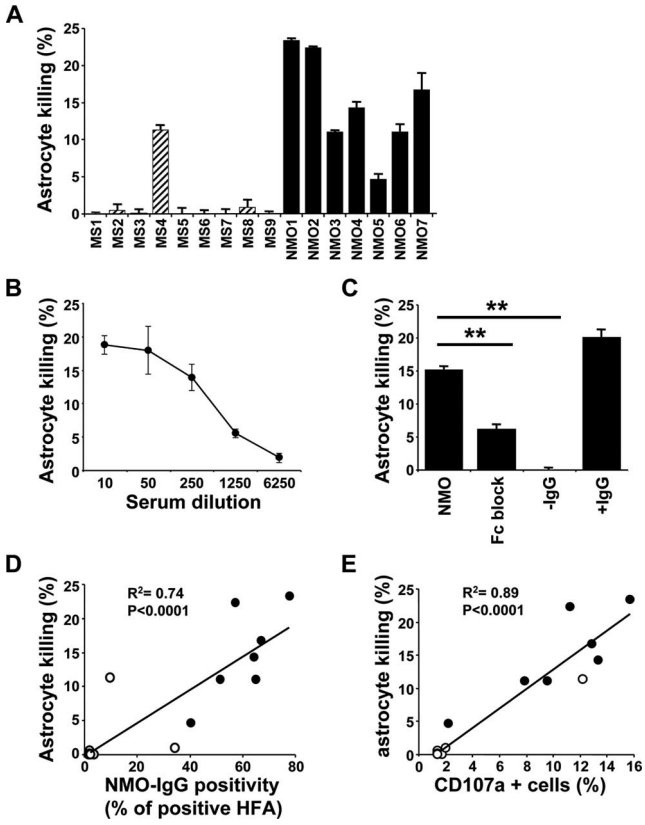

FIGURE 6. HFA-bound NMO-IgGs induce astrocyte killing by ADCC. *A*, The percentage of specific astrocyte killing by NK cells as determined in a 4-h ^{51}Cr release assay in which HFAs were preincubated for 1 h with culture medium containing 10% test serum from seven NMO-IgG-positive (■) and nine sex- and age-matched MS patients (▨). Data shown are mean ± SD of triplicate wells. *B*, Serial dilution assay showing that the NK cell-mediated specific killing of HFAs preincubated with NMO-IgG serum is dose-dependent. Data shown are mean ± SD of triplicate wells. *C*, Inhibition of the specific astrocyte killing by blocking Fc receptors (FcRs) on the NK cells by preincubation with polyclonal human IgG (Fc block) and by serum IgG depletion (−IgG). The NMO-IgG-concentrated eluate fraction (+IgG) restores the specific killing. Data shown are mean ± SD of triplicate wells. **, $p < 0.01$. *D*, Correlation between reactivity of serum IgGs against HFAs (as the percentage of HFAs with bound IgG) and NK cell-mediated killing of HFAs preincubated with NMO-IgG-positive (●) or MS (○) sera. *E*, Correlation between CD107a expression on NK cells and NK cell-mediated astrocyte killing after coculture with HFAs preincubated with NMO-IgG-positive (●) or MS (○) sera.

lower chambers and fluorescent-BSA permeability was measured at different time points over 72 h. Incubation with NMO-IgG sera induced a significant increase in BBB permeability to FITC-BSA at 48 and 72 h compared with MS sera ($p < 0.001$ and $p < 0.001$, respectively; $n = 3$) (Fig. 4*C*).

NMO-IgGs support astrocyte-directed Ab-dependent cellular cytotoxicity (ADCC)

To test whether AQP4 targeting by NMO-IgG could induce ADCC of astrocytes, we assessed the expression of the degranulation marker CD107a on the surface of human NK cells (effector cells) cocultured with HFAs (target cells) in the presence or absence of NMO-IgGs. The FACS profile presented in Fig. 5*A* illustrates the increased percentage of NK cells expressing CD107a following contact with HFAs preincubated with NMO-IgG-positive sera. As shown in Fig. 5, *B* and *C*, we found that sera from six of seven NMO-IgG-positive patients induced significant CD107a surface expression by NK cells compared with only one of nine MS sera ($p < 0.0001$) and none of the four healthy control sera ($p = 0.0002$). We found a correlation between the ability of serum IgGs to bind HFAs (NMO-IgG positivity) (Fig. 3*B*) and their efficiency in inducing NK cell degranulation ($p = 0.0002$) (Fig. 5*D*).

We directly measured the ability of NK cells to kill HFAs in a chromium release assay. After 4 h, preincubation with 10% NMO-IgG-positive sera induced 10 times more NK-mediated astrocyte killing when compared with MS sera (14.7 ± 6.7% vs 1.4 ± 3.7; $p = 0.006$) (Fig. 6*A*). Serial dilution of NMO-IgG serum showed a clear dose response correlation (Fig. 6*B*). This lytic response was inhibited when Fc receptors were saturated by preincubation of NK cells with irrelevant polyclonal human IgG ("Fc block") (6.2 ± 0.75%; $p = 0.002$) (Fig. 6*C*). Furthermore, serum IgG depletion using a Sepharose-protein G column completely suppressed the astrocyte killing (0 ± 0.4%; $p = 0.001$). Conversely, the NMO-IgG-concentrated eluate fraction restored the killing (Fig. 6*C*). Interestingly, the only MS serum able to induce astrocyte killing by NK cells was one of the two sera shown to slightly

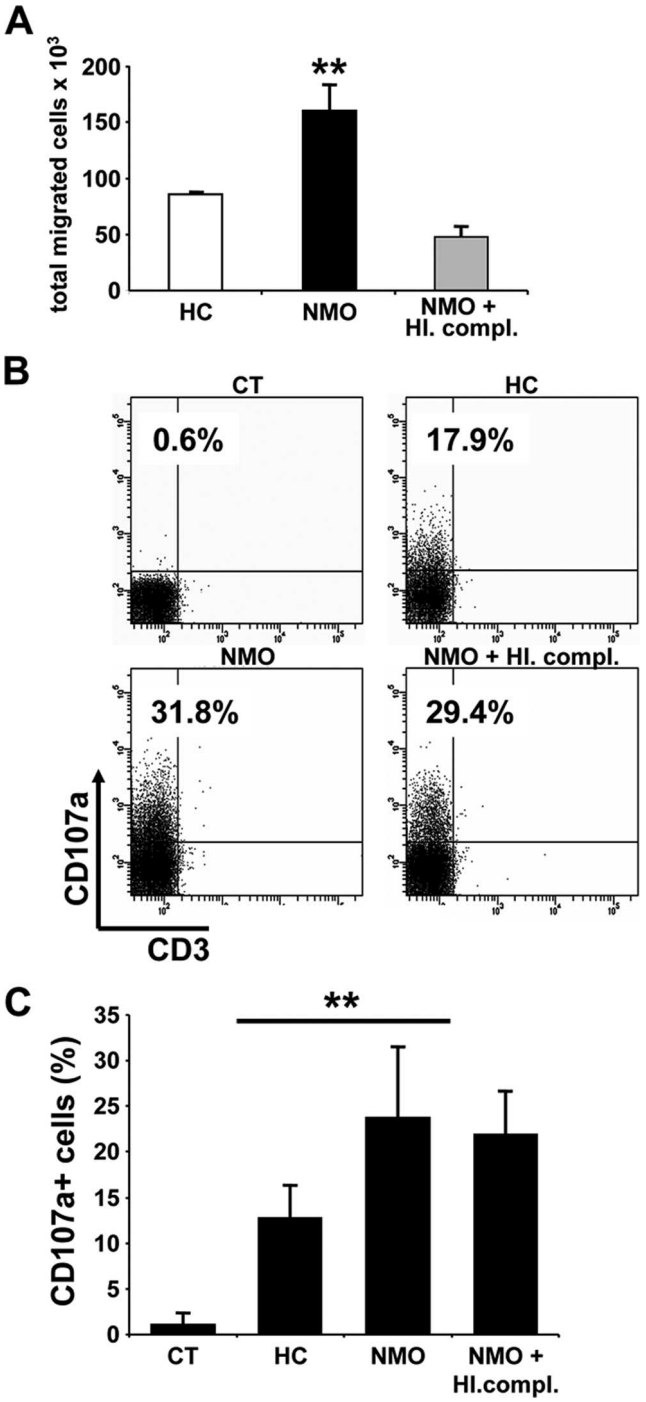

FIGURE 7. NMO-IgGs induce complement-dependent migration and complement-independent degranulation of granulocytes. *A*, Increase in number of granulocytes that migrate through BBB-ECs and enter lower compartment of a Boyden chamber coated with HFAs preincubated with NMO-IgG-positive or health control serum, in presence of fresh or heat-inactivated (HI) complement. Data shown are mean ± SD from three sera samples per group in duplicate. **, $p < 0.01$. *B*, Representative FACS analyses showing an increased percentage of granulocytes (CD3-negative cells) that express CD107a following transmigration across BBB-EC barrier toward HFAs preincubated with NMO-IgG-positive compared with healthy control serum, in presence of fresh or heat-inactivated (HI) complement. The percentage of CD107a-positive cells was not altered by complement heat inactivation. Nonmigrated granulocytes were used as a negative control (CT). *C*, Mean ± SD from three sera samples per group. **, $p < 0.01$.

bind HFAs by FACS analysis (serum MS4) (Figs. 3*B* and 6*A*). We further found a significant positive correlation between serum IgGs binding to HFAs (NMO-IgG positivity) (Fig. 3*B*) and their ability to induce NK-cell mediated astrocyte-directed ADCC ($p < 0.0001$) (Fig. 6*D*). Finally, we demonstrated in this model that cell surface mobilization of CD107a by NK cells is strongly correlated with their cytotoxic activity ($p < 0.0001$) (Fig. 6*E*). We could not induce HFA lysis by incubation of the cells only with NMO-IgG containing serum and fresh serum as a source of complement (data not shown), suggesting that effector cells are required in situ to propagate Ab-dependent cytotoxicity of astrocytes.

NMO-IgG induces complement-dependent granulocyte migration across the BBB

To examine whether NMO-IgG binding to astrocytes would lead to complement-dependent granulocyte attraction, we used a BBB-EC-coated Boyden chamber based assay in which the bottom chamber contained HFAs preincubated with either NMO-IgG-positive or healthy control sera together with fresh serum as a source of complement. Granulocytes were added to the upper chamber and allowed to migrate across BBB-ECs for 2 h. Compared with healthy control sera, HFAs preincubated with NMO-IgG-positive sera induced a significant increase in granulocyte migration through BBB-ECs (total migrated cells = $86 \times 10^3 \pm 1.7 \times 10^3$ and $161 \times 10^3 \pm 23 \times 10^3$ respectively; $p < 0.01$) (Fig. 7*A*). Heat inactivation of the serum inhibited the chemoattraction induced by NMO-IgGs (total migrated cells = $48 \times 10^3 \pm 10 \times 10^3$; $p = 0.001$) (Fig. 7*A*). Granulocytes that had migrated toward NMO-IgG-incubated HFAs exhibited increased CD107a mobilization compared with migration toward HFAs incubated with healthy control sera (percentage of CD107a-positive cells = 23.8 ± 8.9 and 12.8 ± 4.8 respectively; $p < 0.01$) (Fig. 7, *B* and *C*). Although complement inactivation inhibited granulocyte attraction, it did not suppress their degranulation (percentage of CD107a-positive cells = 22 ± 5.8) (Fig. 7*C*), indicating that granulocyte degranulation was not related to complement activation, but rather to the contact with NMO-IgG-coated astrocytes at the bottom of the well.

Discussion

We initiated our study by identifying sera, obtained from NMO and longitudinally extensive transverse myelitis patients, which showed in situ immunoreactivity using primate cerebellar slices. The vasculocentric pattern of immunoreactivity obtained was similar to that previously reported in studies using rodent cerebellar tissue sections and to that obtained using anti-AQP4 Ab (2, 3). We used these sera to demonstrate that NMO-IgGs bind to primary human astrocytes in vitro. We further show that NMO-IgGs have functional effects on the cellular components of the neurovascular unit, promoting BBB opening and granulocyte recruitment, both of which are features of NMO.

CNS microvasculature ECs need constant input from the glial cells to maintain their BBB-related properties (22, 23). Our data suggest at least two different ways by which interaction of NMO-IgGs with astrocytes could alter BBB function. The first would be to interfere with AQP4 expression or function. To test this hypothesis we used HFA/BBB-EC cocultures as a model of BBB. In these cocultures, astrocytes present long processes with AQP4 molecules concentrated at their end-feet, reproducing the polarized expression at the BBB seen in situ. This polarized expression was completely disrupted after incubation with NMO-IgG-containing sera; these sera seemed to induce AQP4 internalization, similarly to a phenomenon observed by Lennon and colleagues (24) using non-neural tissue-derived cell lines. As AQP4 is known to regulate water fluxes in the brain, it was likely that this altered expression

would influence BBB permeability. Accordingly, altered BBB integrity associated with hyperpermeability has been observed in AQP4 knockout mice (6). To directly test this hypothesis, we cultured HFAs and BBB-ECs on alternate sides of a Boyden chamber membrane and found that NMO-IgG-containing sera induce a significant increase in BBB permeability. AQP4 has recently been implicated in the adhesion and the migration of astrocytes providing additional potential mechanisms by which AQP4 internalization could alter BBB integrity (25–27). These direct effects of NMO-IgGs on the neurovascular unit could account for the relatively rapid clinical efficacy of plasma exchanges when used to treat NMO (7–9).

We then explored a second mechanism by which AQP4 targeting by NMO-IgGs could promote a breach in the neurovascular unit, by sensitizing astrocytes for ADCC. As a proof of principle for these studies, we used NK lymphocytes as the effectors, as these cells are known to secrete cytotoxic granules and be mediators of ADCC following Fc receptor engagement. Although the exact influence of NK cells in the development of NMO lesion has not been defined, presence of Fc receptor bearing effector cells (e.g., macrophage-microglia, granulocytes) within NMO lesions is well known (28). Our data confirm that when NK cells are cocultured with HFAs in the presence of NMO-IgGs, NK cells degranulate, as measured by expression of surface CD107a, and astrocyte death ensues. Taken together, our findings are consistent with neuropathological features of NMO demonstrating necrotic inflammatory lesions associated with a loss of AQP4 and GFAP immunoreactivity, vasculocentric deposition of immune complexes, and macrophage-microglia activation (12, 13, 29, 30). We did not observe any binding of NMO sera IgGs with AQP4 negative cells such as neurons and mature oligodendrocytes (data not shown). We found a strong correlation between the ability of serum IgGs to bind HFAs as assessed by FACS analysis, and the capability of the serum to potentiate ADCC, demonstrating the functional relevance of this assay. When NMO-IgG were quantified by indirect immunofluorescence, we did not find a significant correlation between immunohistochemical reactivity and HFA binding or NK cell degranulation (data not shown), suggesting that our FACS assay reflect more closely the functional potential of NMO-IgG than the classical immunofluorescence assay. However, we did not observe astrocyte cytotoxicity of NMO-IgGs along with complement, in the absence of cellular effectors. This observation is consistent with previous studies showing astrocyte resistance to complement-induced lysis, due to their membrane expression of complement regulatory proteins (31).

We further used the astrocyte/BBB-EC BBB coculture model to demonstrate that astrocyte-bound NMO-IgGs may be involved in granulocyte recruitment, another pathologic feature that discriminates NMO lesions from typical MS lesions (32). We observed increased granulocyte recruitment only in the presence of a source of fresh complement. This event could be related to the release of chemotactic factors, i.e., the anaphylatoxins C3a and C5a, in the classical complement activation pathway. C5a is a chemoattractant for neutrophils and eosinophils, whereas C3a is a chemotaxin for eosinophils and can stimulate neutrophils cells after eosinophil activation (33). Consistently, a recent study has demonstrated that transgenic expression of C3a in the CNS markedly exacerbates experimental autoimmune encephalomyelitis and results in massive perivascular recruitment of inflammatory cells to the spinal cord (34). The tetrameric structure of AQP4 molecules favors IgG oligomerization, making NMO-IgG-coated astrocyte membranes ideal surfaces for complement classical pathway activation leading to release of C3a and C5a fragments and consequently, increase in microvascular permeability and granulocyte chemo-attraction. Although we observed CD107a mobilization on granulocytes after their migration through the BBB, this degranulation was not prevented by complement inactivation suggesting that this response was mediated by direct contact with the Ab-coated astrocytes. Although ADCC has been described with polymorphonuclear cells (35), we failed to demonstrate significant cytotoxicity of granulocytes on NMO-IgG-coated HFAs even at high E:T ratio (our unpublished data). However, it is likely that the release of hydrolytic granular enzymes, bioactive lipids, and superoxide anions after granulocyte degranulation could contribute to brain injury (36).

In conclusion, we provide experimental demonstration of the pathogenic mechanism by which serum-derived NMO-IgGs induce CNS necrotic lesion formation. We have demonstrated that HFA-bound NMO-IgGs are able to induce 1) decreased AQP4 expression on astrocyte end-feet and increased BBB permeability, 2) NK cell degranulation and astrocyte killing by ADCC, and 3) complement-dependent granulocyte attraction through the BBB. These data bring new physiopathological explanations for BBB breakdown, loss of AQP4 immunoreactivity, and perivascular granulocyte infiltration described in active NMO lesions. A better understanding of the physiopathological processes underlying NMO lesion formation should help the development of therapies for this severe and disabling disease.

Acknowledgments

We thank Nathalie Arbour and Salvatore Carbonetto for highly stimulating discussion. We thank M. Blain and M. Bernard for excellent technical assistance in the laboratory and all the clinical staff involved in this study.

Disclosures

The authors have no financial conflict of interest.

References

1. Wingerchuk, D. M., V. A. Lennon, C. F. Lucchinetti, S. J. Pittock, and B. G. Weinshenker. 2007. The spectrum of neuromyelitis optica. *Lancet Neurol.* 6: 805–815.
2. Lennon, V. A., D. M. Wingerchuk, T. J. Kryzer, S. J. Pittock, C. F. Lucchinetti, K. Fujihara, I. Nakashima, and B. G. Weinshenker. 2004. A serum autoantibody marker of neuromyelitis optica: distinction from multiple sclerosis. *Lancet* 364: 2106–2112.
3. Lennon, V. A., T. J. Kryzer, S. J. Pittock, A. S. Verkman, and S. R. Hinson. 2005. IgG marker of optic-spinal multiple sclerosis binds to the aquaporin-4 water channel. *J. Exp. Med.* 202: 473–477.
4. Nicchia, G. P., B. Nico, L. M. Camassa, M. G. Mola, N. Loh, R. Dermietzel, D. C. Spray, M. Svelto, and A. Frigeri. 2004. The role of aquaporin-4 in the blood-brain barrier development and integrity: studies in animal and cell culture models. *Neuroscience* 129: 935–945.
5. Verkman, A. S., D. K. Binder, O. Bloch, K. Auguste, and M. C. Papadopoulos. 2006. Three distinct roles of aquaporin-4 in brain function revealed by knockout mice. *Biochim. Biophys. Acta* 1758: 1085–1093.
6. Zhou, J., H. Kong, X. Hua, M. Xiao, J. Ding, and G. Hu. 2008. Altered blood-brain barrier integrity in adult aquaporin-4 knockout mice. *Neuroreport* 19: 1–5.
7. Keegan, M., A. A. Pineda, R. L. McClelland, C. H. Darby, M. Rodriguez, and B. G. Weinshenker. 2002. Plasma exchange for severe attacks of CNS demyelination: predictors of response. *Neurology* 58: 143–146.
8. Watanabe, S., I. Nakashima, T. Misu, I. Miyazawa, Y. Shiga, K. Fujihara, and Y. Itoyama. 2007. Therapeutic efficacy of plasma exchange in NMO-IgG-positive patients with neuromyelitis optica. *Mult. Scler.* 13: 128–132.
9. Weinshenker, B. G., P. C. O'Brien, T. M. Petterson, J. H. Noseworthy, C. F. Lucchinetti, D. W. Dodick, A. A. Pineda, L. N. Stevens, and M. Rodriguez. 1999. A randomized trial of plasma exchange in acute central nervous system inflammatory demyelinating disease. *Ann. Neurol.* 46: 878–886.
10. Lucchinetti, C. F., R. N. Mandler, D. McGavern, W. Bruck, G. Gleich, R. M. Ransohoff, C. Trebst, B. Weinshenker, D. Wingerchuk, J. E. Parisi, and H. Lassmann. 2002. A role for humoral mechanisms in the pathogenesis of Devic's neuromyelitis optica. *Brain* 125: 1450–1461.
11. Pittock, S. J., B. G. Weinshenker, C. F. Lucchinetti, D. M. Wingerchuk, J. R. Corboy, and V. A. Lennon. 2006. Neuromyelitis optica brain lesions localized at sites of high aquaporin 4 expression. *Arch. Neurol.* 63: 964–968.
12. Roemer, S. F., J. E. Parisi, V. A. Lennon, E. E. Benarroch, H. Lassmann, W. Bruck, R. N. Mandler, B. G. Weinshenker, S. J. Pittock, D. M. Wingerchuk, and C. F. Lucchinetti. 2007. Pattern-specific loss of aquaporin-4 immunoreactivity distinguishes neuromyelitis optica from multiple sclerosis. *Brain* 130: 1194–1205.

13. Misu, T., K. Fujihara, A. Kakita, H. Konno, M. Nakamura, S. Watanabe, T. Takahashi, I. Nakashima, H. Takahashi, and Y. Itoyama. 2007. Loss of aquaporin 4 in lesions of neuromyelitis optica: distinction from multiple sclerosis. *Brain* 130: 1224–1234.
14. Takahashi, T., K. Fujihara, I. Nakashima, T. Misu, I. Miyazawa, M. Nakamura, S. Watanabe, Y. Shiga, C. Kanaoka, J. Fujimori, et al. 2007. Anti-aquaporin-4 antibody is involved in the pathogenesis of NMO: a study on antibody titre. *Brain* 130: 1235–1243.
15. D'Souza, S., K. Alinauskas, E. McCrea, C. Goodyer, and J. P. Antel. 1995. Differential susceptibility of human CNS-derived cell populations to TNF-dependent and independent immune-mediated injury. *J. Neurosci.* 15: 7293–7300.
16. Wosik, K., B. Becher, A. Ezman, J. Nalbantoglu, and J. P. Antel. 2001. Caspase 8 expression and signaling in Fas injury-resistant human fetal astrocytes. *Glia* 33: 217–224.
17. Prat, A., K. Biernacki, B. Becher, and J. P. Antel. 2000. B7 expression and antigen presentation by human brain endothelial cells: requirement for proinflammatory cytokines. *J. Neuropathol. Exp. Neurol.* 59: 129–136.
18. Stanimirovic, D., A. Shapiro, J. Wong, J. Hutchison, and J. Durkin. 1997. The induction of ICAM-1 in human cerebromicrovascular endothelial cells (HCEC) by ischemia-like conditions promotes enhanced neutrophil/HCEC adhesion. *J. Neuroimmunol.* 76: 193–205.
19. Rubio, V., T. B. Stuge, N. Singh, M. R. Betts, J. S. Weber, M. Roederer, and P. P. Lee. 2003. Ex vivo identification, isolation and analysis of tumor-cytolytic T cells. *Nat. Med.* 9: 1377–1382.
20. Saikali, P., J. P. Antel, J. Newcombe, Z. Chen, M. Freedman, M. Blain, R. Cayrol, A. Prat, J. A. Hall, and N. Arbour. 2007. NKG2D-mediated cytotoxicity toward oligodendrocytes suggests a mechanism for tissue injury in multiple sclerosis. *J. Neurosci.* 27: 1220–1228.
21. Ifergan, I., K. Wosik, R. Cayrol, H. Kebir, C. Auger, M. Bernard, A. Bouthillier, R. Moumdjian, P. Duquette, and A. Prat. 2006. Statins reduce human blood-brain barrier permeability and restrict leukocyte migration: relevance to multiple sclerosis. *Ann. Neurol.* 60: 45–55.
22. Brillault, J., V. Berezowski, R. Cecchelli, and M. P. Dehouck. 2002. Intercommunications between brain capillary endothelial cells and glial cells increase the transcellular permeability of the blood-brain barrier during ischaemia. *J. Neurochem.* 83: 807–817.
23. Prat, A., K. Biernacki, K. Wosik, and J. P. Antel. 2001. Glial cell influence on the human blood-brain barrier. *Glia* 36: 145–155.
24. Hinson, S. R., S. J. Pittock, C. F. Lucchinetti, S. F. Roemer, J. P. Fryer, T. J. Kryzer, and V. A. Lennon. 2007. Pathogenic potential of IgG binding to water channel extracellular domain in neuromyelitis optica. *Neurology* 69: 2221–2231.
25. Auguste, K. I., S. Jin, K. Uchida, D. Yan, G. T. Manley, M. C. Papadopoulos, and A. S. Verkman. 2007. Greatly impaired migration of implanted aquaporin-4-deficient astroglial cells in mouse brain toward a site of injury. *FASEB J.* 21: 108–116.
26. McCoy, E., and H. Sontheimer. 2007. Expression and function of water channels (aquaporins) in migrating malignant astrocytes. *Glia* 55: 1034–1043.
27. Nicchia, G. P., M. Srinivas, W. Li, C. F. Brosnan, A. Frigeri, and D. C. Spray. 2005. New possible roles for aquaporin-4 in astrocytes: cell cytoskeleton and functional relationship with connexin43. *FASEB J.* 19: 1674–1676.
28. Jarius, S., F. Paul, D. Franciotta, P. Waters, F. Zipp, R. Hohlfeld, A. Vincent, and B. Wildemann. 2008. Mechanisms of disease: aquaporin-4 antibodies in neuromyelitis optica. *Nat. Clin. Pract. Neurol.* 4: 202–214.
29. Misu, T., K. Fujihara, M. Nakamura, K. Murakami, M. Endo, H. Konno, and Y. Itoyama. 2006. Loss of aquaporin-4 in active perivascular lesions in neuromyelitis optica: a case report. *Tohoku J. Exp. Med.* 209: 269–275.
30. Satoh, J. I., S. Obayashi, T. Misawa, H. Tabunoki, T. Yamamura, K. Arima, and H. Konno. 2008. Neuromyelitis optica/Devic's disease: Gene expression profiling of brain lesions. *Neuropathology*. In press.
31. Spiller, O. B., G. Moretto, S. U. Kim, B. P. Morgan, and D. V. Devine. 1996. Complement expression on astrocytes and astrocytoma cell lines: failure of complement regulation at the C3 level correlates with very low CD55 expression. *J. Neuroimmunol.* 71: 97–106.
32. Wingerchuk, D. M., V. A. Lennon, S. J. Pittock, C. F. Lucchinetti, and B. G. Weinshenker. 2006. Revised diagnostic criteria for neuromyelitis optica. *Neurology* 66: 1485–1489.
33. Daffern, P. J., P. H. Pfeifer, J. A. Ember, and T. E. Hugli. 1995. C3a is a chemotaxin for human eosinophils but not for neutrophils. I. C3a stimulation of neutrophils is secondary to eosinophil activation. *J. Exp. Med.* 181: 2119–2127.
34. Boos, L., I. L. Campbell, R. Ames, R. A. Wetsel, and S. R. Barnum. 2004. Deletion of the complement anaphylatoxin C3a receptor attenuates, whereas ectopic expression of C3a in the brain exacerbates, experimental autoimmune encephalomyelitis. *J. Immunol.* 173: 4708–4714.
35. Horner, H., C. Frank, C. Dechant, R. Repp, M. Glennie, M. Herrmann, and B. Stockmeyer. 2007. Intimate cell conjugate formation and exchange of membrane lipids precede apoptosis induction in target cells during antibody-dependent, granulocyte-mediated cytotoxicity. *J. Immunol.* 179: 337–345.
36. Henson, P. M. 1971. The immunologic release of constituents from neutrophil leukocytes. I. The role of antibody and complement on nonphagocytosable surfaces or phagocytosable particles. *J. Immunol.* 107: 1535–1546.